Journal of Neurochemistry

JNC

JOURNAL OF NEUROCHEMISTRY | 2017 | 143 | 595–608

doi: 10.1111/jnc.14216

ORIGINAL ARTICLE

Functional changes in the neural retina occur in the absence of mitochondrial dysfunction in a rodent model of diabetic retinopathy

Dustin R. Masser,*,†,‡ Laura Otalora,*,‡,§ Nicholas W. Clark,*,‡ Michael T. Kinter,§,¶ Michael H. Elliott** and Willard M. Freeman*,†,‡,§

*Department of Physiology, The University of Oklahoma Health Sciences Center, Oklahoma City, Oklahoma, USA

†Harold Hamm Diabetes Center, The University of Oklahoma Health Sciences Center, Oklahoma City, Oklahoma, USA

‡Reynolds Oklahoma Center on Aging, Oklahoma City, Oklahoma, USA

§Oklahoma Nathan Shock Center on Aging, Oklahoma City, Oklahoma, USA

¶Aging & Metabolism Program, Oklahoma Medical Research Foundation, Oklahoma City, Oklahoma, USA

**Department of Ophthalmology, The University of Oklahoma Health Sciences Center, Oklahoma City, Oklahoma, USA

Abstract

Diabetic retinopathy is a neurovascular diabetes complication resulting in vision loss. A wealth of literature reports retinal molecular changes indicative of neural deficits, inflammation, and vascular leakage with chronic diabetes, but the mechanistic causes of disease initiation and progression are unknown. Microvascular mitochondrial DNA (mtDNA) damage leading to mitochondrial dysfunction has been proposed to drive vascular dysfunction in retinopathy. However, growing evidence suggests that neural retina dysfunction precedes and may cause vascular damage. Therefore, we tested the hypothesis that neural mtDNA damage and mitochondrial dysfunction are an early initiating factor of neural diabetic retinopathy development in a rat streptozotocin-induced, Type I diabetes model. Mitochondrial function (oxygen consumption rates) was quantified in retinal synaptic terminals from diabetic and non-diabetic rats with paired retinal structural and function assessment (optical coherence tomography and electroretinography, respectively). Mitochondrial genome damage was assessed by identifying mutations and deletions across the mtDNA genome by high depth sequencing and absolute mtDNA copy number counting through digital PCR. Mitochondrial protein expression was assessed by targeted mass spectrometry. Retinal functional deficits and neural anatomical changes were present after 3 months of diabetes and prevented/normalized by insulin treatment. No marked dysfunction of mitochondrial activity, maladaptive changes in mitochondrial protein expression, alterations in mtDNA copy number, or increase in mtDNA damage was observed in conjunction with retinal functional and anatomical changes. These results demonstrate that neural retinal dysfunction with diabetes begins prior to mtDNA damage and dysfunction, and therefore retinal neurodegeneration initiation with diabetes occurs through other, non-mitochondrial DNA damage, mechanisms.

Keywords: diabetes, diabetic retinopathy, insulin, mitochondria, mtDNA, retina.

J. Neurochem. (2017) **143**, 595–608.

Received July 26, 2017; revised manuscript received August 24, 2017; accepted September 6, 2017.

Address correspondence and reprint requests to Willard M. Freeman, Department of Physiology, The University of Oklahoma Health Sciences Center, SLY-BRC 1370, 975 NE 10th St, Oklahoma City, OK 73104, USA. E-mail: wfreeman@ouhsc.edu

Abbreviations used: BHMTC, Benjamini-Hochberg Multiple Testing Correction; COXIV, cytochrome c oxidase subunit IV; D+I, diabetic with insulin replacement; D, diabetic; DMMC, Dunn's Method Multiple Comparisons; dPCR, digital PCR; DR, diabetic retinopathy; ERG, electroretinography; FCCP, carbonyl cyanide-4-trifluoromethoxy phenylhydrazone; mtDNA, mitochondrial DNA; ND, non-diabetic; OCR, oxygen consumption rate; OCT, optical coherence tomography; ONL, outer nuclear layer; OP, oscillatory potentials; PBST, phosphate buffered saline with tween; qPCR, quantitative PCR; R/AA, rotenone/antimycin a; ROS, reactive oxygen species; SNK, Student Newman Keuls; STZ, streptozotocin; TCA, tricarboxylic acid cycle.

Diabetic retinopathy (DR) is a neurovascular secondary complication of diabetes that affects the retina, the light-sensitive neural tissue of the posterior eye. While the majority of Type 1 diabetic patients experience some form of vision loss attributed to DR, the etiology of DR and pathophysiological progression remain elusive (Stitt *et al.* 2016). The combination of inflammation, neurodegeneration, and vascular leakage present clinically likely forms a feed-forward cycle causing tissue dysfunction (Antonetti *et al.* 2006). Recent evidence supports the idea that neurodegeneration may be the initial insult, setting this cycle in motion (Sohn *et al.* 2016; Lynch and Abramoff 2017). Early vision deficits are neural in origin and occur in the absence of angiogenesis and other vascular hallmarks of DR (Jackson *et al.* 2012; Sohn *et al.* 2016). Diligent glycemic control is a proven approach for DR prevention, but aggressive insulin replacement therapy is often insufficient to prevent disease development (Aiello and Group 2014; Nathan *et al.* 2015). Treatments aimed at halting neovascularization and angiogenesis are promising for preserving remaining vision in late-stage proliferative DR (Vaziri *et al.* 2015), but likely have limited utility as preventative treatments for diabetic patients. Thus, there is the opportunity to identify the initial/early DR mechanisms, prior to the development of proliferative retinopathy, which could be targeted in combination with glycemic control to prevent DR disease process initiation. Previously we reported loss of synaptic connections and synaptic proteins within the inner and outer plexiform layers as well as dysregulation of gene expression starting at around 1 month of uncontrolled diabetes (VanGuilder *et al.* 2008; Bixler *et al.* 2011). These neural changes occur before vascular dysfunction and increased permeability (Brucklacher *et al.* 2008; Bixler *et al.* 2011; VanGuilder *et al.* 2011; Masser *et al.* 2014). This sequence of neural changes prior to overt vascular dysfunction is also evident clinically (Lorenzi and Gerhardinger 2001; Gardner *et al.* 2002; Sennlaub *et al.* 2003; Sohn *et al.* 2016). However, the initiating causes of the neural retina DR disease process and neurodegeneration remain unclear.

In the retinal vasculature, extended, uncontrolled diabetes results in mitochondrial deficits including mitochondrial DNA (mtDNA) damage, presumably mutations and deletions, as a result of oxidative damage (Kowluru and Abbas 2003; Kowluru and Mishra 2015). mtDNA are circular genomes present in multiple copies in the inner mitochondrial matrix that encode only necessary subunits of the electron transport chain in addition to rRNA and tRNA for localized mRNA translation (Taylor and Turnbull 2005). Mitochondria are critical for proper neural tissue function by providing cellular energy in the form of ATP through glycolysis, and calcium storage and buffering necessary for proper synaptic transmission (Sheng and Cai 2012; Dupuis 2014). Therefore, mtDNA mutations have the potential to disrupt neural function and result in a loss of mitochondrial homeostasis with diabetes. mtDNA damage and mitochondrial function have been assessed previously, albeit with qualitative methods, after long durations (> 6 months) of uncontrolled experimental diabetes with the interpretation that damaged mitochondria in retinal endothelial cells drive DR initiation and progression (Madsen-Bouterse *et al.* 2010; Zhong and Kowluru 2011; Santos *et al.* 2012; Tewari *et al.* 2012). However, the nature and degree of mtDNA damage and functional deficits in the diabetic neural retina is unknown. The scientific premise of this study is: the neural retina damage evident early in diabetes may be mediated by mitochondrial dysfunction. This is supported by the findings that long-term diabetes causes mitochondrial dysfunction in non-neural cells of the retina, and in other retinal diseases neural mitochondrial dysfunction induces neurodegeneration (Barot *et al.* 2011). Therefore, we sought to examine mitochondrial function and quantify neural mtDNA damage in a rat model (Freeman *et al.* 2010) at a time point where neuronal changes are occurring but prior to vascular dysfunction (VanGuilder *et al.* 2008; Masser *et al.* 2014). Novel quantitative molecular techniques, mtDNA sequencing and absolute copy number, were used to rigorously assess this scientific premise. Chronic insulin treatment was examined to determine if a standard approach to glycemic control could prevent or normalize any changes observed. We hypothesized that neural retinal mitochondria would be dysfunctional and mtDNA damaged with diabetes at a time where neural retina functional and structural deficits are evident. In this study, retinal function and morphology were measured in experimental diabetic rats, and subsequently a quantitative assessment of mitochondrial respiration, mtDNA damage, mtDNA copy number, and mitochondrial protein expression from retinal synaptosomes were performed.

Methods

Animals

Rats were housed from birth in a dimly lit pathogen-free environment at the Dean McGee Eye Institute Animal Facility, and maintained in accordance with Institutional Animal Care and Use Committee guidelines (IACUC approval #101379-15-101-HC). Light intensity on the top and bottom housing racks were equal. Water and food were provided *ad-libitum* throughout the study, unless otherwise stated. Sprague-Dawley (RRID: RGD_5508397) breeder pairs were purchased from Charles River. ANOVA power analysis was performed assuming alpha of 0.5, minimum difference of 10% and standard deviation of 5% with three experimental groups and minimal sample size of six gives a power of 0.812. A total of 12 animals per group were therefore chosen to provide more than sufficient power even in the event of loss of animals to humane endpoints. Two cohorts of male rat pups were weaned at 7 days, ear tagged, and placed in cages with littermates (n = 36/cohort [N = 72]). Data include animals from both cohorts combined, unless otherwise stated. At ~1.5 months of age (~150–250 g), rats were fasted overnight and weighed. Randomization into treatment groups was carried out using block randomization to ensure equal experimental groups (Suresh 2011). A single intraperitoneal

injection of streptozotocin (STZ, at 65 mg/kg, Sigma Aldrich, Saint Louis, MO, USA) dissolved in 10 mM sodium citrate (pH 4.5) was administered to 24 rats in each cohort as previously described (VanGuilder *et al.* 2008; Bixler *et al.* 2011; Masser *et al.* 2014). Aged-matched non-diabetic controls received a single equal volume intraperitoneal injection of sodium citrate buffer. Diabetes induction was confirmed 1 week post-injection and only STZ-injected animals with non-fasted blood glucose measurements ≥ 250 mg/dL (groups were blinded from the tester) were retained. This resulted in 93% conversion, or 7% of animals failing diabetes induction. Additionally, animals were excluded if they lost > 15% body mass over two consecutive weeks. This resulted in three diabetic animals euthanized before the termination of the study. The unconverted animals and animals that were euthanized early for humane endpoints were excluded from all study endpoints. All animals were euthanized humanely by decapitation under pentobarbital anesthesia (100 mg/kg) administered by a single intraperitoneal injection.

Blood glucose and glycated hemoglobin

Starting 1 week post-STZ or sodium citrate vehicle injection blood glucose levels were measured from a drop of blood from a lancet tail-nick (Lifescan One-touch Meter; Johnson & Johnson) (Masser *et al.* 2014) bi-weekly for diabetic rats and non-diabetic controls and weekly for insulin-treated diabetic rats. At euthanasia, glycated hemoglobin (HbA1c) levels were measured from a drop of blood collected by lancet tail-nick using monoclonal antibody agglutination immunoassay cartridges and a DCA analyzer (PTS Diagnostics) (Masser *et al.* 2014).

Insulin administration

A subset of diabetic rats (n = 12/cohort) received insulin replacement beginning 6 weeks post-STZ injection by subcutaneous implantation (26 mg human insulin pellet, 7 × 2 mm; LinShin Canada) via trocar under transient isoflurane vapor anesthesia. These insulin pellets provide a continual dose of 2U of insulin per 24 h for the duration for the pellet. Endogenous rat c-peptide and exogenous human insulin levels were measured by enzyme-linked immunosorbent assays (Mercodia) (Masser *et al.* 2014) using plasma collected from trunk blood at the time of euthanization.

Electroretinography and optical coherence tomography

One week prior to euthanasia (12–13 weeks diabetes duration), rats were assessed for retinal function by electroretinography (ERG). Rats were weighed and dark adapted for 12 h overnight prior to ERG recording. Preparation of the rats is described in detail in the Supplemental Methods. A ColorDome and Espion E3 ERG instrument (Diagnosys LLC) was used to stimulate and record responses. The 11 step protocol consisted of a zero stimulus for removing the baseline trace, then a 6 step serial scotopic range of −4.87 log cd*s/m^2 to −1.4 log cd*s/m^2, and finally a 4 step photopic series ranging from 0.34 log cd*s/m^2 to 1.3 log cd*s/m^2 paired with a rod suppressing background illumination (10 cd/m^2) to isolate cone function. Oscillatory potentials (OP) were recorded for both scotopic and photopic readings using a digital filter of 75–300 Hz on virtual channels. Raw data from right and left eyes were isolated for each rat from scotopic and photopic measurement stimuli and responses were averaged for each rat. Time to peak for each OP was isolated and averaged per group.

Retinal thickness was measured using optical coherence tomography (OCT) (Bioptigen SD OCT Envisu R4300, Leica Microsystems, Wetzlar, Germany) immediately following ERG recording. OCT images were analyzed manually via Bioptigen InVivoVue Diver Software 2.4 (Leica Microsystems). A 5 × 5 grid retinal template was used for depth analysis centered on the optic nerve head for each image. Measurements from each layer were averaged across eyes from each animal (Figure S1).

Synaptosome isolation

Retinal synaptosomes were isolated as previously described (VanGuilder *et al.* 2008) with modifications. Right and left retinas were excised, combined per animal, and placed in 15 mL of ice-cold sucrose buffer (0.32 M sucrose, 4 mM HEPES, 1 mM sodium orthovanadate, pH to 7.4). Retinas were homogenized by mechanical dounce homogenization in 3 mL of ice-cold sucrose buffer (approximately 10–15 strokes) and centrifuged at 4°C (Optima L-80 XP ultracentrifuge, SW32.1 Ti swinging bucket, Beckman Coulter, Brea, CA, USA) 800 g for 10 min to pellet nuclei and large cell fragments. Supernatants were decanted into a clean ultracentrifuge tube and placed on ice and pellets saved. Supernatant fractions were centrifuged at 4°C and 25 000 g for 12 min to pellet synaptosomes. Pellets were maintained on ice for subsequent use.

Oxygen consumption rate measurement

Oxygen consumption rates (OCR) for retinal synaptosomes were measured by Seahorse XFe96 extracellular flux analyzer and XF Cell Mito Stress Test (Agilent, Santa Clara, CA, USA) as outlined previously (Choi *et al.* 2009) with modifications and according to manufacturer's instructions. Isolated retinal synaptosome pellets from each animal were resuspended in 300 μL ionic media (20 mM HEPES, 10 mM D-glucose, 1.2 mM disodium phosphate, 1 mM magnesium chloride, 5 mM sodium bicarbonate, 140 mM sodium chloride, pH to 7.4), and 9 μL of the resuspended synaptosomes were aliquoted (20 μg of protein/well quantified after OCR measurements) in duplicate or triplicate wells containing 50 μL of ice-cold ionic media. Oligomycin, FCCP (Carbonyl cyanide-4-trifluoromethoxy phenylhydrazone), and antimycin A/rotenone drugs were dissolved and diluted in incubation media to final assay well concentrations of 1 μM oligomycin, 2 μM FCCP, and 1 μM rotenone/antimycin a (R/AA). All steps of the Seahorse run protocol were performed at 37°C.

Immunoblot and mass spectrometry

Protein was isolated from Seahorse microplate wells and pellet fractions. Immuno dot-blots were performed using cytochrome c oxidase subunit IV (COXIV) primary antibody [1 : 1000 in 5% bovine serum albumin (BSA), COXIV, (abcam, Cambridge, United Kingdom) RRID: AB_301443]. COXIV dot-blot intensities were determined by densitometry using ImageQuant (GE, RRID: SCR_014246) image analysis software. Immunoblots were performed using Lamin B1 (1 : 5000 in 5% non-fat dry milk, Lamin B1, (abcam, RRID: AB_2616597), COXIV (1 : 1000 in 5% BSA, COXIV, abcam) RRID: AB_301443), and synaptophysin (1 : 500 in 5% BSA, synaptophysin, abcam, RRID: AB_2198854) antibodies, and visualized using horseradish peroxidase (HRP)-conjugated secondary antibodies (1 : 1000 in 5% BSA, HRP-conjugated goat anti-mouse, (Rockland, Pottstown, PA, USA) RRID: AB_2610851;

1 : 1000 in 5% BSA, HRP-conjugated rabbit anti-rabbit, Rockland, RRID: AB_2610848) and X-ray film exposure.

Mass spectrometry of retinal synaptosomes was carried out as previously described (Nakada *et al.* 2017). The analyses were carried out on a TSQ Vantage triple quadrupole mass spectrometry system (ThermoFisher, Waltham, MA, USA). The HPLC was an Eksigent splitless nanoflow system (Eksigent, Dublin, CA, USA) with a 10 cm × 75 μm i.d. C18 reversed phase capillary column. The mass spectrometer was operated in the selected reaction monitoring mode. Data were analyzed using SkyLine to determine the integrated peak area of the appropriate chromatographic peaks. The response for each protein was calculated as the geometric mean of the two peptide area. These values were normalized to the response for the BSA standard in pmol/100 μg total protein.

Nucleic acid isolation

DNA and RNA were co-isolated as previously described (Masser *et al.* 2013, 2016) using silica-spin column purification according to manufacturer's instructions (Zymo Research, Irvine, CA, USA). Isolated DNA and RNA was qualified and preliminarily quantified by spectrophotometry (NanoDrop, ThermoFisher), and precisely quantified by fluorometric assay (PicoGreen, ThermoFisher).

Sequencing standard generation

Total genomic rat DNA isolated from two rats with germline base differences at four known locations on the mitochondrial genome. A common forward primer and two reverse primers were used to amplify short and long mtDNA fragments (Table S1) containing the base differences. mtDNA amplicons were ligated into vectors (TOPO TA, Life Technologies, Grand Island, NY, USA), transformed into competent *E.coli*. (One Shot TOP10, Life Technologies). Colonies were picked and grown in super optimal broth (SOB) medium. Plasmids were isolated using silica-spin column purification (Zymo Research) and sequence identity of inserts confirmed by Sanger sequencing.

mtDNA copy number quantitation

mtDNA was absolutely quantified (copies per ng input DNA) by digital PCR by methods we previously developed (Masser *et al.* 2016) using a custom mtDNA TaqMan primer-probe copy number assay (RnMtDNA_CCI1MPG, ThermoFisher).

mtDNA sequencing and analysis

mtDNA was amplified using 1 ng total DNA and long-range proofreading PCR (TaKaRa LR DNA Polymerase) with primers specific for the mitochondrial genome (Table S1). 500 pg of mtDNA amplicon per sample were used for sequencing library preparation with Nextera XT reagents (Illumina , San Diego, CA, USA) similar to previously described (Masser *et al.* 2013). Libraries were diluted to 4 nM and pooled for MiSeq benchtop next generation sequencing (Illumina) using 600 cycle (2 × 250 bp) reagents (Illumina) at a final library concentration of 12 pM. Detailed bioinformatics analysis methods are provided in the Supplemental Methods.

Statistics

Statistical analyses were carried out in Sigma Plot 12.5 (Systat Software, San Diego, CA, USA). Parametric One-Way ANOVA S with Student-Newman-Keuls post-hoc testing, were performed on data passing equal variance and normality testing (Shapiro-Wilk), while non-parametric analyses, Kruskal-Wallis One-Way ANOVA on Ranks with Dunn's *post-hoc*, were carried out on data not meeting equal variance and normality. Significance was set to $\alpha = 0.05$. P-values were corrected for multiple comparisons as appropriate with a false-discovery rate of $q < 0.2$ (Benjamini and Hochberg 2000).

Results

Longitudinal blood glucose and body weight monitoring

Time course of treatments and endpoints is detailed in Fig. 1a. Hyperglycemia (blood glucose ≥ 250 mg/dL) in diabetic (D) animals was confirmed at 1 week post STZ injection and in comparison, blood glucose in age-matched non-diabetic (ND) controls were normal (< 140 mg/dL) (Fig. 1b). Diabetic animals that received insulin replacement (D+I) received subcutaneous insulin pellets starting 6 weeks post-STZ injection. Blood glucose dropped to ND control levels in D+I rats and was maintained by subsequent insulin pellet implants when blood glucose levels reached > 250 mg/dL (Fig. 1b). At the end of the study, blood glucose levels were equivalent in ND and D+I animals, while D animals had significantly higher blood glucose levels compared to ND and D+I animals (Table S2). Body mass was also measured longitudinally. ND animals gained weight, while D animal growth was stunted (Fig. 1c). Once diabetic animals received insulin, body mass increased, indicative of insulin action and a resumed growth pattern. At the end of the study, ND and D+I animal weights were significantly greater compared to D animals (Table S2). These differences in blood glucose and body weights were consistent across both animal cohorts.

Insulin and HbA1c

Glycated hemoglobin (HbA1c) levels were significantly higher in D animals compared to ND controls (Table S2) and in D+I animals compared to ND controls, indicative of the initial 6 week period of hyperglycemia, however, they were also significantly lower as compared to D animals (D vs. D+I $p < 0.05$), indicative of improved glycemic control. In addition to blood glucose levels, diabetes induction was confirmed at the end of the study by measuring serum levels of rat c-peptide, a marker of endogenous insulin production. ND animals had significantly higher c-peptide levels compared to D and D+I (Table S2). C-peptide levels were equivalent in D and D+I animals, demonstrating similar levels of pancreatic β-cell depletion with STZ treatment. HbA1c and c-peptide differences were consistent across both animal cohorts. Serum from D+I animals were positive for human insulin, confirming delivery from the insulin pellets (Table S2).

Retinal morphology and function

Structural morphology of retinal cell layers was assessed 1 week prior to the conclusion of the study using non-

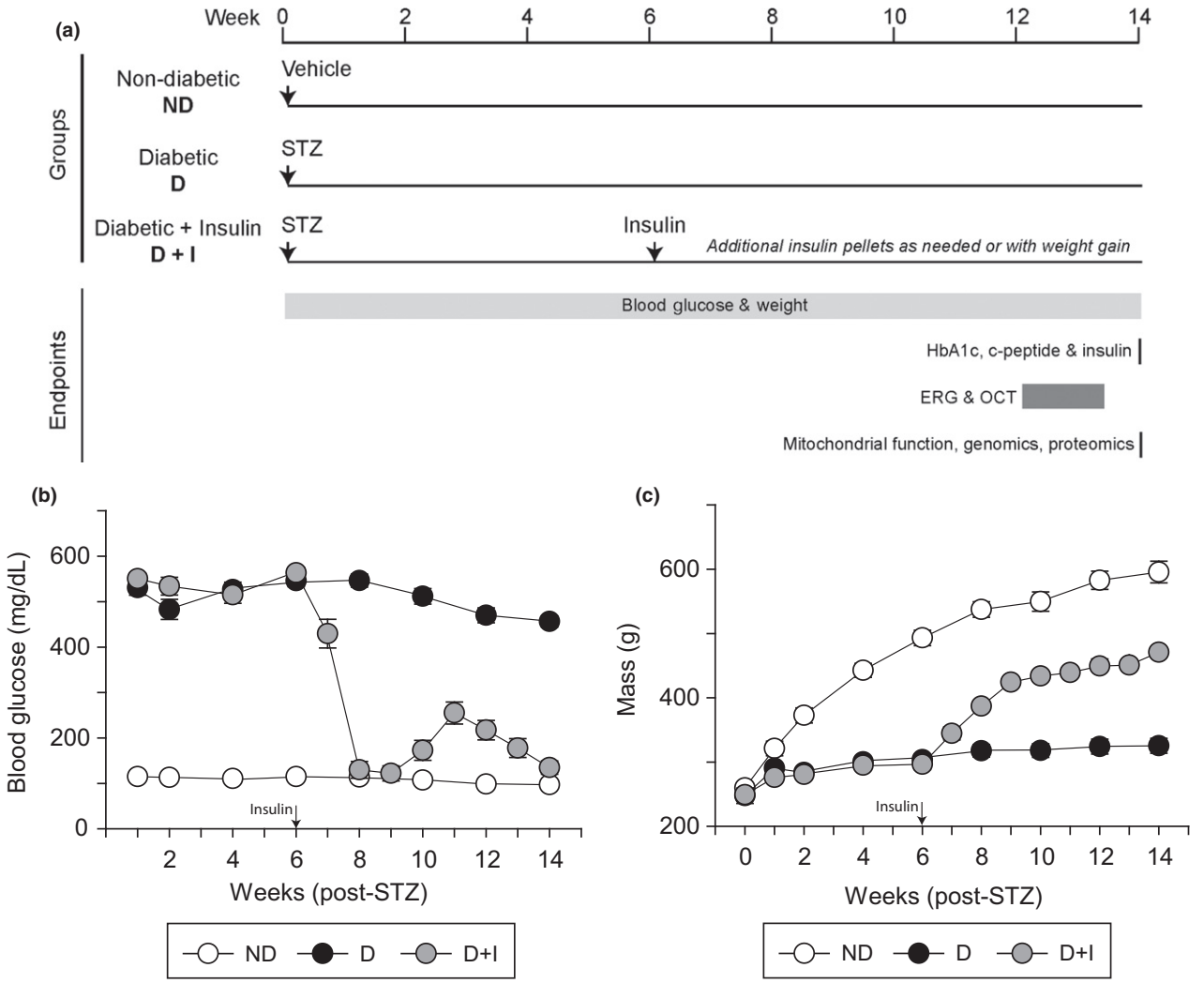

Fig. 1 Longitudinal blood glucose and body mass monitoring. (a) Experimental design and timeline of data acquisition. Electroretinography (ERG) and optical coherence tomography (OCT) were performed 12–13 weeks post-STZ, while physiological, molecular, and biochemical end-points were measured 14 weeks post-STZ. (b) Weekly B blood glucose monitoring (mg/dL) for the duration of the study (weeks post-streptozotocin (STZ) or vehicle injection) in non-diabetic (ND – white circles), diabetic (D – black circles), and diabetic with insulin replacement (D+I – gray circles) animals. Insulin administration was begun 6 weeks post-STZ injection (arrow). (c) Body mass monitoring (g – grams) for the duration of the study before STZ injection (week 0) and for the subsequent study weeks in ND (white circles), D (black circles), and D+I (gray circles) animals. Arrow indicates when D+I animals received insulin implants. n = 16–22 animals/group. Error bars – standard error of the mean.

invasive optical coherence tomography (OCT), which allows for the quantitative measurement of retinal layer morphology. Representative retinal cross section images (middle data point of the 5 × 5 grid) from each experimental group are shown in Fig. S1. In D animals, the outer nuclear layer (ONL) was significantly thicker compared to ND controls (Table S3). D+I animals also had a significantly thicker ONL compared to ND controls, however, D+I animals had a significantly thinner ONL compared to D animals. Additionally, D and D+I animals had a significantly thinner retinal pigmented epithelium compared to ND controls (Table S3). The ganglion cell layer, inner plexiform layer, inner nuclear layer, outer plexiform layer, and photoreceptor layer were not significantly altered with diabetes. In total, diabetes did not significantly alter total retinal thickness (Table S3).

Retinal neuronal function was measured by electroretinography (ERG) in dark-(scotopic) and light-adapted (photopic) conditions to assess rod and cone channels, respectively. Scotopic flash intensities were low (see methods)(Pardue *et al.* 2014), and elicited only a minor a-wave response. Therefore, the final scotopic intensity (-1.4 log cd s/m^2) was used to compare a-wave amplitudes across experimental groups, rather than the intensity-response relationship. The scotopic a-wave amplitude at this flash intensity was

significantly attenuated in D animals compared to ND controls (Table S4) but a-wave implicit time was not. The scotopic b-wave maximal amplitude, half-maximal stimulus intensity and b-wave implicit time were not significantly altered with diabetes (Table S4). Scotopic oscillatory potentials (OPs) implicit times were significantly longer in D animals compared to ND controls as demonstrated by representative traces of OP responses from the scotopic −1.4 log(cd s/m^2) stimulus (Fig. 2a). Comparison of mean implicit times of OP1 through OP4 peaks were significantly longer in D animals for each OP compared to ND controls (Fig. 2b). OPs measured from D+I animals demonstrated an intermediate phenotype with OP1 mean implicit time normalized to ND control levels (Fig. 2b). OP2 mean implicit time was significantly shorter in D+I animals compared to D animals, but was significantly higher compared to ND animals (Fig. 2b). OP3 and OP4 mean implicit times in D+I animals were not significantly different from either D or ND controls.

For photopic ERG responses, there were no significant differences with diabetes in a- or b-wave implicit times and mean amplitudes (Table S4). Photopic OP implicit times were not different for the first OP as show in representative traces (Fig. S2a). However, OP2 and OP3 implicit times demonstrated small, but significant, delays in implicit time (Figure S2b). In the D+I animals there were no significant differences in OP implicit time compared to either the ND controls or the D animals, demonstrating a partial normalization with insulin replacement (Fig. S2b).

Mitochondrial respiratory function

In order to quantify mitochondrial function, OCR were measured from isolated retinal synaptosomes by extracellular flux analysis (Fig. 3) and normalized to the protein expression of Cytochrome c oxidase subunit IV (COXIV). Synaptosomes were isolated from the rest of the retina and enriched for mitochondria (Fig. S3). Oxygen consumption attributed to basal respiration, ATP production, non-ATP respiration, maximal respiration, spare respiratory capacity, and non-mitochondrial respiration was quantified through the use of sequential pharmacological inhibitors to components of the electron transport chain (Fig. 3a and b). Basal OCR was significantly higher in D and D+I animals compared to ND controls (Fig. 3c). Additionally, ATP-linked OCR was significantly higher in D and D+I animals compared to ND controls (Fig. 3d). However, diabetes did not alter OCRs of non-ATP linked respiration (Fig. 3e), maximal respiration (Fig. 3f), spare respiration capacity (Fig. 3g), or non-mitochondrial respiration (Fig. 3h).

Antioxidant/beta oxidation/Krebs cycle protein quantification

The quantitative expression of 100 proteins directly related to antioxidant status, beta oxidation, and the Krebs/tricarboxylic acid (TCA) cycle was carried out on retinal synaptosome protein by mass spectrometry using a panel of known peptides specific to each protein target (n = 6/group) (Fig. 4a) (Nakada *et al.* 2017). Proteins are listed in Table S5. The housekeeping protein Hspd1 was quantified and demonstrated no group differences (Table S5). Seven of the antioxidant-related proteins were found to be significantly different across groups. Five of these proteins (Pygm, Gsta3, Msra, Pygb, Prdx1) were significantly increased in the D animals compared to ND controls. Pc was significantly decreased in D animals compared to controls (Fig. 4b). With the exception of Pc, proteins that were significantly increased with diabetes returned to ND control levels or were significantly lower than D animals in the D+I animals (Fig. 4b). Three beta oxidation-related proteins (Acot13, Hadhb, Acsl1) were significantly increased in the D animals compared to ND controls and were subsequently normalized in the D+I animals (Fig. 4c). Furthermore, none of the TCA/Krebs cycle proteins were significantly differentially expressed with diabetes. However, of the proteins that passed multiple testing corrections (Slc25a11, Sucgl1, Etfb, Sdhb, Idh3a, Echs1, Idh3 g, Idh3b) all were significantly decreased in expression in the D+I animals compared to D or ND controls (Fig. 4d).

Absolute quantitation of mitochondrial DNA copy number

To assess if mitochondrial DNA (mtDNA) copy number in isolated retinal synaptic mitochondria decreased with diabetes, absolute mtDNA number was quantified by digital PCR (dPCR) (Masser *et al.* 2016). There were no differences in the number of mtDNA genomes present in retinal synaptosomes across the groups (Fig. 5a). Furthermore, mtDNA copy number was quantified from whole retinal DNA isolated from an independent animal cohort presented in our previous report (Masser *et al.* 2014) and no difference in mtDNA copies in D or D+I animals compared to ND controls was observed (Fig. S4). Differences in absolute levels are because of the inclusion of nuclear DNA in the whole retinal samples that is absent in the synaptosome preparations and represents the bulk of the DNA mass in a cell.

mtDNA sequencing

In order to quantify and map mtDNA damage in the form of large deletions and somatic single nucleotide variants with diabetes, high-depth mtDNA sequencing was performed. Positive controls and quantitative determination of method sensitivity for detection of large deletions and single nucleotide variant frequencies was performed using *in vitro* generated sequencing standards with and without known deletions and variants (File S1 and Fig. S5a) mixed at known ratios resulting in standard curves for variants and deletions ranging from 0% to 100% deleted/variant frequency. Single nucleotide variants were quantified at the expected variant

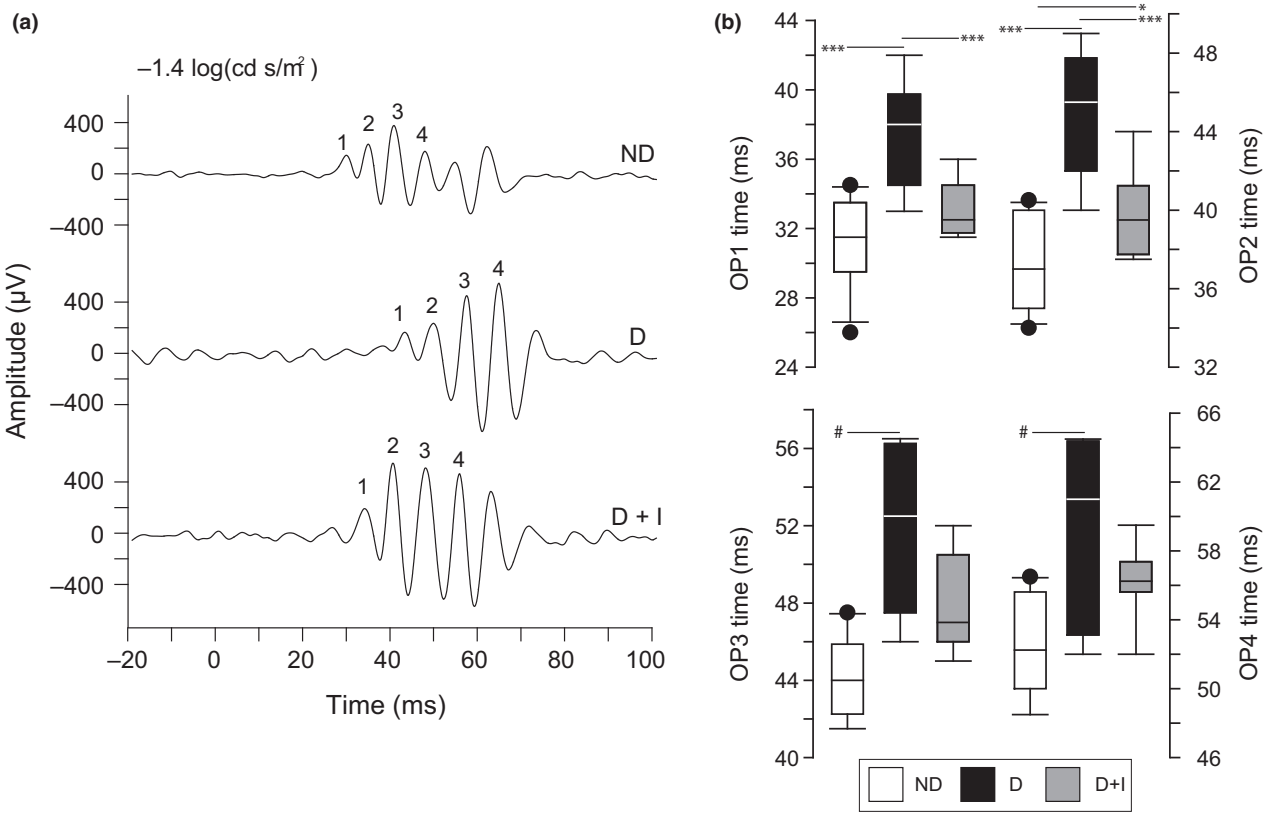

Fig. 2 Electroretinogram (ERG) scotopic oscillatory potentials (OP) 12-13 weeks post-STZ injection. (a) Representative OP traces from non-diabetic (ND – top), diabetic (D – middle), and diabetic with insulin replacement (D+I – bottom) animals showing amplitude (μV) and time (ms) after dark-adapted light stimulus [−1.4 log(cd s/m^2)] at time 0. Numbers (1–4) mark the OPs used for mean and individual implicit time comparison between experimental groups (OP1, OP2, OP3, and OP4). (b) Scotopic OP mean implicit time group comparisons for OP1, OP2, OP3, and OP4 between ND (white), D (black), and D+I (gray) animals. *$p < 0.05$, ***$p < 0.001$, One-Way ANOVA with Student-Newman-Keuls Method, n = 9–11 animals/group. $^{\#}p < 0.05$, Kruskall-Wallis One-Way ANOVA on Ranks with Dunn's Method, n = 9–11 animals/group).

frequencies (Fig. S5b and Table S6). Large-scale deletions were identified in the form of gapped reads and were found at the expected frequencies relative to the '100% deleted' sequencing standard (Fig. S5c and Table S6). These validation experiments demonstrate that somatic deletions and single nucleotide variants can be quantitatively detected down to frequencies of 0.1% through this deep sequencing approach.

Sequencing was performed on 15 848 bp of the mtDNA genome (primer binding regions were excluded) from base pairs 223–16 121 (Table S1) of the rat reference mtDNA genome. Average mapped reads per sample was 335 790 in ND controls (n = 10), 357,827 in D controls (n = 7), and 317,457 in D+I animals (n = 10), and the average depth of coverage was 1757 ± 1395, 1837 ± 615, and 1712 ± 1394, respectively. No differences in the number of mtDNA deletions between the groups (Fig. 5b) were observed in synaptosomal samples. A comprehensive, quantitative analysis of somatic mitochondrial genome variants identified a number of low frequency mutations in every animal (Fig. 5c). The total variant frequency per base-pair of the mtDNA (sum of variant frequency/number of variants/15848 bp) was not significantly different when assessing all called variants. Examining only those variants that would cause an amino acid change, or only silent variants (Table S7) revealed no differences between groups. Additionally, variants present in the coding regions of each annotated mitochondrially encoded gene were assessed. No significant differences in variant frequencies (sum of variants frequency across the annotation/number of variants/length of gene in basepairs) (Fig. 5g) across any gene regions were detected between experimental groups (Table S7). Re-running retinal synaptosome mtDNA sequencing at higher sequencing depths and sequencing mtDNA from whole retinas also demonstrate no differences in variant frequencies or deletions with diabetes (Figures S6 and S7, Tables S8 and S9). Results for these sequencing runs are presented in detail in the Supplemental Material.

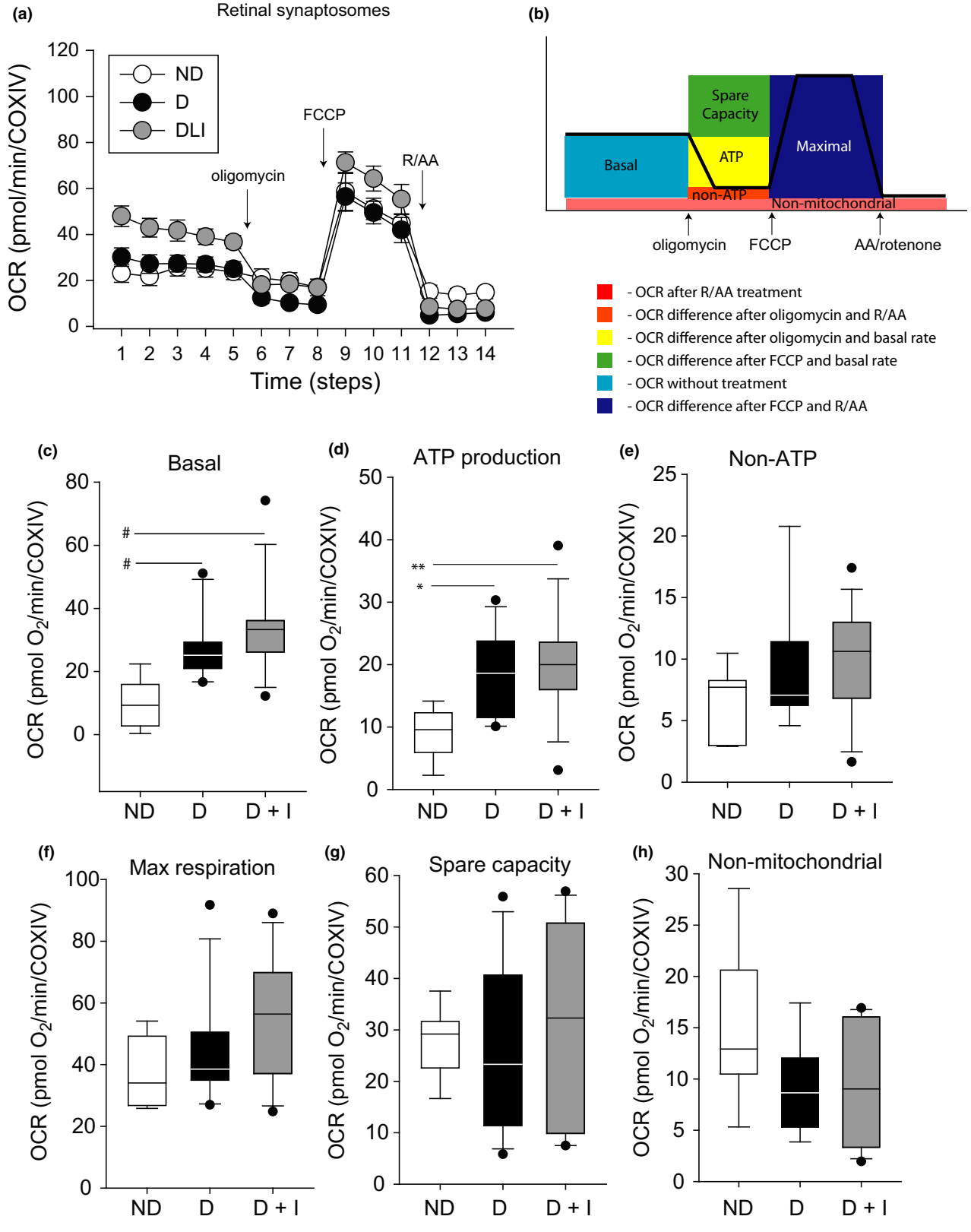
(a)
Retinal synaptosomes
OCR (pmol/min/COXIV)
ND
D
DLI
oligomycin
FCCP
R/AA
Time (steps)
(b)
Spare Capacity
Basal
ATP
Maximal
non-ATP
Non-mitochondrial
oligomycin
FCCP
AA/rotenone
- OCR after R/AA treatment
- OCR difference after oligomycin and R/AA
- OCR difference after oligomycin and basal rate
- OCR difference after FCCP and basal rate
- OCR without treatment
- OCR difference after FCCP and R/AA
(c)
Basal
(d)
ATP production
(e)
Non-ATP
(f)
Max respiration
(g)
Spare capacity
(h)
Non-mitochondrial
OCR (pmol O2/min/COXIV)
ND
D
D + I

Fig. 3 Mitochondrial oxygen consumption measurements from retinal synaptosomes 14 weeks post-STZ injection. Normalized mean oxygen consumption rates (OCR) of isolated retinal synaptosomes from non-diabetic (ND), diabetic (D), and diabetic with insulin replacement (D+I). (a) Oxygen consumption rate (OCR) over time with sequential pharmacological inhibitors from isolated retinal synaptosomes. Non-diabetic (ND – white), diabetic (D – black), and diabetic with insulin replacement (D+I – gray) animals (n = 10–13 animals/group). Arrows indicate when drug [oligomycin, FCCP, or rotenone/antimycin A (R/AA)] were added. (b) Schematic of OCR experiment demonstrating components of the OCR curve attributed to the consumption rate. Oligomycin inhibits complex V, which blocks ATP production, and the loss of oxygen consumption can be attributed to ATP-linked respiration. FCCP uncouples the proton gradient and ATP production of the inner-mitochondrial membrane allowing protons to freely pass into the inner-mitochondrial matrix which disrupts the membrane potential. In response, respiration is increased to re-establish the proton gradient and membrane potential giving a measure of maximal respiratory capacity. Finally, the combination of antimycin A, which inhibits complex III, and rotenone, which inhibits complex I, blocks mitochondrial respiration completely, and the subsequent oxygen consumption is a result of respiration independent of mitochondria. Error bars – standard error of the mean. (c) Basal OCR (d) OCR linked to ATP production (e) OCR from non-ATP (f) OCR from maximal respiration (g) Spare capacity OCR and (h) non-mitochondrial OCR. $*p < 0.05$, $**p < 0.01$, One-Way ANOVA with Student-Newman-Keuls Method, n = 10–13 animals/group, $^{\#}p < 0.05$, Kruskall-Wallis One-Way ANOVA on Ranks with Dunn's Method, Benjamini Hochberg Multiple Testing Correction, n = 10–13 animals/group). COXIV – cytochrome c oxidase subunit IV protein expression.

Discussion

This study demonstrates that diabetic changes in neural retinal morphology and function occur within 3 months, are partially normalized/prevented by systemic insulin treatment, and confirms a number of studies demonstrating early neuronal retinal dysfunction with diabetes (Aung *et al.* 2013; Pardue *et al.* 2014; Sohn *et al.* 2016). Critically, no quantitative changes in mitochondrial function, protein expression, or mtDNA integrity, indicative of mitochondrial dysfunction or damage, occur in the neural retina over this timeframe as determined by novel quantitative approaches to assay the mitochondrial genome directly. These findings provide strong evidence that diabetic mitochondrial dysfunction is not a causative factor in the initial neural retina response.

These findings are contrary to our hypothesis and suggest a difference between the neural retina and retinal vasculature where studies demonstrate endothelial mitochondrial dysfunction as an initiating factor of vascular dysfunction (Kowluru and Abbas 2003; Madsen-Bouterse and Kowluru 2008; Madsen-Bouterse *et al.* 2010; Zhong and Kowluru 2011; Santos *et al.* 2012; Tewari *et al.* 2012; Kowluru and Mishra 2015). No significant deficits in challenged mitochondrial activity were quantified with diabetes at a time point where neural retinal deficits are present. Increased expression of mitochondrial-related beta oxidation and antioxidant proteins with diabetes, indicates a cellular response to systemic hyperglycemia in the retina, but is likely a positively adaptive response. These results are similar to a previous demonstration of protective, positively adaptive mitochondrial protein activity changes in response to short-term diabetes (Osorio-Paz *et al.* 2015), which results in decreased mitochondrial efficiency but not dysfunction. Base and location specific quantitative assessment of retinal mtDNA damage in the form of somatic deletions and mutations across multiple high-depth mitochondrial sequencing datasets demonstrate that no induction of deletions or mutations occurs with early diabetes. This form of mitochondrial sequencing has not been previously applied to DR research and provides a new level of specificity and quantitation to this analysis. Absolute quantification of retinal mtDNA copy number using dPCR also demonstrates no differences with diabetes. Taken together, our data show that neural retinal functional and morphological changes in early diabetes occur without mitochondrial dysfunction or mtDNA damage. The neural function and anatomy studies provide further validation of the STZ-rat DR model and demonstrates that in addition to developing the similar molecular phenotypes as DR patients (Brucklacher *et al.* 2008; Freeman *et al.* 2010; VanGuilder *et al.* 2011; Masser *et al.* 2014), this model has early neural functional (Aung *et al.* 2013; Pardue *et al.* 2014) and morphological changes (VanGuilder *et al.* 2008; Masser *et al.* 2014; Sohn *et al.* 2016) and shares commonalities with non-proliferative diabetic retinopathy patients (Abcouwer and Gardner 2014).

While our results and interpretation do not support the hypothesis that mitochondrial dysfunction is causative of neural DR initiation and early progression, our findings are buttressed by the threshold effect concept in mitochondrial biology (Durham *et al.* 2007; Stewart and Chinnery 2015). The threshold effect is the idea that mtDNA damage must pass a critical frequency threshold within a mitochondrion/cell in order for that damage to biochemically and functionally alter the mitochondrion. Put simply, the relationship of mtDNA mutation and deletion rates to impaired mitochondrial function is not linear. In diseases and model systems where mutations or deletions of mtDNA cause functional impairments, mtDNA damage reaches frequencies of greater than 60% before a functional phenotype is present (Stewart and Chinnery 2015). Therefore, if mtDNA damage causes mitochondrial dysfunction in the retina with diabetes and these events initiate the hallmarks of vascular leakage, inflammation, and neurodegeneration observed early with DR, the mtDNA damage induced by diabetes would need to be several orders of magnitude greater than the < 0.02% frequency observed here. A recent study using mtDNA sequencing data collected from exome sequencing within the

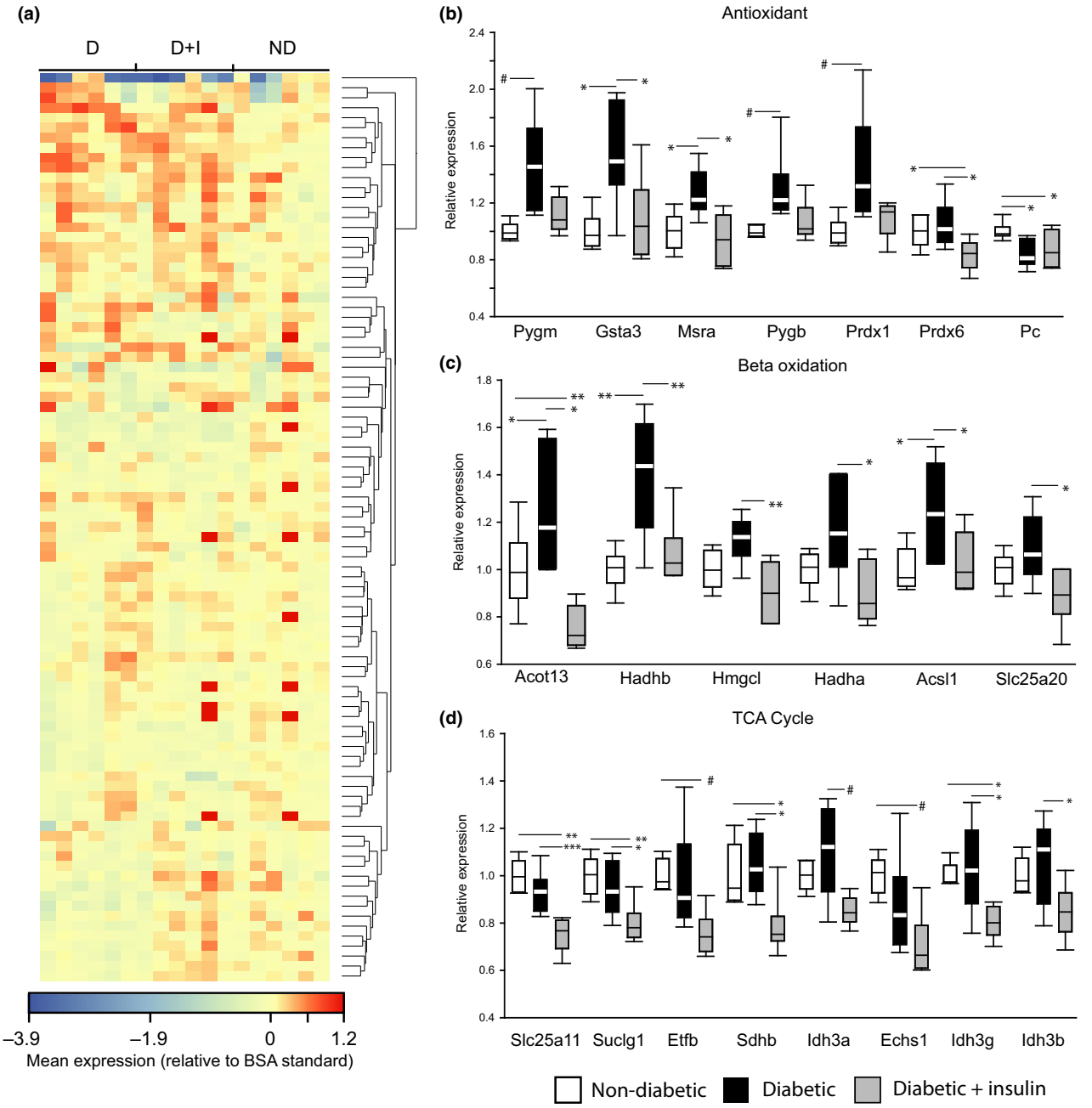

Fig. 4 Mass spectrometry quantitation of mitochondrial proteins 14 weeks post-STZ injection. (a) Heatmap (mean expression relative to BSA standard) of (b) antioxidant, (c) beta oxidation, and (b) tricarboxylic acid cycle (TCA)/Krebs cycle proteins quantified from isolated retinal synaptosomes in non-diabetic (ND), diabetic (D), and diabetic with insulin replacement (D+I) animals. $*p < 0.05$, $**p < 0.01$, $***p < 0.001$, One-way ANOVA with Student-Newman-Keuls Method, Benjamini Hochberg Multiple Testing Correction, $n = 6$ animals/group. $^{\#}p < 0.05$, One-Way ANOVA on Ranks with Dunn's Method, $n = 6$ animals/group. Pygm – glycogen phosphorylase, muscle associated. Gsta3 – glutathione s-transferase alpha 3. Msra- methionine sulfoxide reductase A. Pygb – glycogen phosphorylase, brain associated. Prdx1 – peroxiredoxin 1. Prdx6 – peroxiredoxin 6. Pc – pyruvate carboxylase. Acot13 – acyl-coa thioesterase 13. Hadhb – hydroxyacyl-coA dehydrogenase beta. Hmgcl – 3-hydroxymethyl-3-methylglutaryl-coA lyase. Hadha – hydroxyacyl-coA dehydrogenase alpha. Acsl1 – acyl-coA synthetase long-chain family member 1. Slc25a20 – Solute carrier family 25 member 20. Slc25a11 – solute carrier family 25 member 11. Suclg1 – succinate-CoA ligase alpha subunit. Etfb – electron transfer flavoprotein beta subunit. Sdhb – succinate dehydrogenase complex iron sulfur subunit b. Idh3a – isocitrate dehydrogenase 3 (NAD+) alpha. Echs1 – enoyl-CoA hydratase, short chain 1. Idh3 g – isocitrate dehydrogenase 3 (NAD+) gamma. Idh3b – isocitrate dehydrogenase 3 (NAD+) beta.

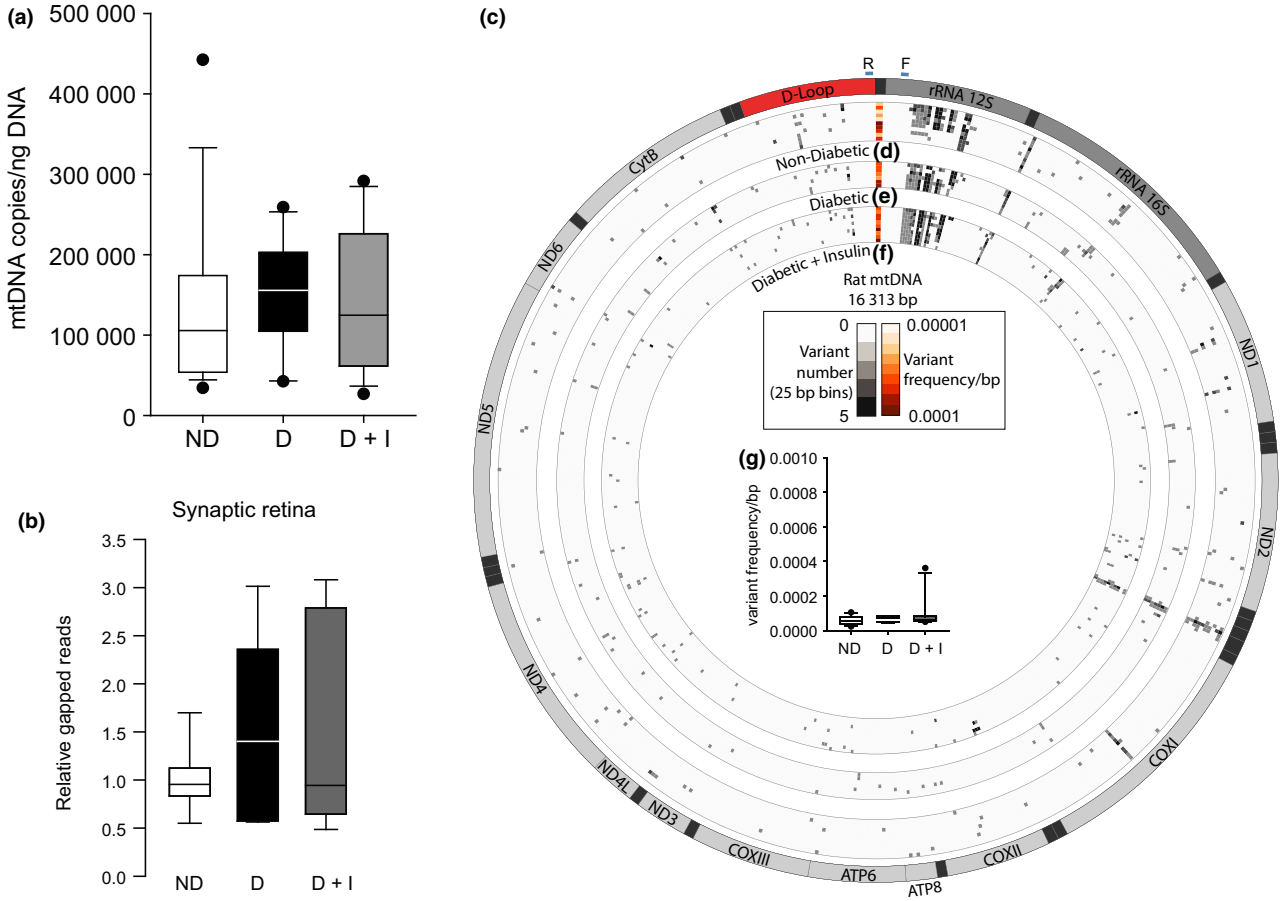

Fig. 5 Mitochondrial genomics 14 weeks post-STZ injection. (a) mtDNA absolute copy number was determined from isolated retinal synaptosomes from non-diabetic (ND), diabetic (D), and diabetic with insulin replacement (D+I) animals normalized to ng of DNA. n = 13–18 animals/group. (b) Relative mtDNA deletion amounts were determined by gapped reads. ND, animals, ratio of gapped/total mapped reads from diabetic (D) and diabetic with insulin replacement (D+I) from mtDNA sequencing from DNA isolated retinal synaptosomes. (c) Ideogram of the 16 313 basepair (bp) mtDNA genes and annotations; dark gray – ribosomal RNA genes, red – D-Loop region, light gray – protein coding genes, and black – tRNAs. Blue regions 'F' and 'R' represent forward and reverse primer binding regions. (d) Number of base variants relative to genomic location of mtDNA per non-diabetic control animal (heatmap rows – gray scale). The single column heatmap represents the mean variant frequency total across the mtDNA for each control animal (total mean variant frequency/bp – orange scale) (n = 10 animals). (e) Number of base variants relative to genomic location of mtDNA per diabetic control animal (heatmap rows – gray scale). The single column heatmap represents the mean variant frequency total across the mtDNA (total mean variant frequency/bp – orange scale) (n = 7 animals). (f) Number of base variants relative to genomic location of mtDNA per diabetic with insulin animal (heatmap rows – gray scale). The single column heatmap represents the mean variant frequency total across the mtDNA (total mean variant frequency/bp – orange scale) (n = 10 animals). (g) Box-plot representation of the mean variant frequency/bp per experimental group. ND- non-diabetic, D – diabetic, D+I – diabetic with insulin replacement. ND1 – NADH dehydrogenase subunit 1. ND2 – NADH dehydrogenase subunit 2. COXI – cytochrome c oxidase subunit 1. COXII – cytochrome c oxidase subunit 2. ATP8 – ATP synthase Fo subunit 8. ATP6 – ATP synthase Fo subunit 6. COX III – cytochrome c oxidase subunit 3. ND3 – NADH dehydrogenase subunit 3. ND4L – NADH dehydrogenase subunit 4L. ND4 – NADH dehydrogenase subunit 4. ND5 – NADH dehydrogenase subunit 5. ND6 – NADH dehydrogenase subunit 6. CytB – cytochrome b.

1000 Genomes Project, found that low frequency variants occurred across a majority of control, non-disease subjects (Ye *et al.* 2014). These data support the validity of our experimental data demonstrating the same observation in our ND controls. Another recent report detailed the effects of mutagens on the mtDNA and found no increased rates of point mutations and deletions after mutagen treatment (Valente *et al.* 2016). These data suggest that adduct formation on the mtDNA is not be as readily converted to somatic variants as previously hypothesized.

These data also address a knowledge gap in the field regarding assessment of mtDNA damage with DR. Most prior reports have not demonstrated mtDNA damage directly, but have concluded damage is the initiator of DR (Kowluru and Abbas 2003; Madsen-Bouterse and Kowluru 2008; Madsen-Bouterse *et al.* 2010; Zhong and Kowluru 2011;

Santos *et al.* 2012; Tewari *et al.* 2012; Kowluru and Mishra 2015). The methods used have been qualitative assays, such as densitometric analysis of long versus short PCR products potentially indicative of mtDNA deletions or adducts. These approaches are not quantitative, are prone to error (Barchiesi *et al.* 2017), and do not determine the base location in the mitochondrial genome of the purported mutations/deletions. The quantitatively validated approaches of dPCR and deep sequencing (massively paralleled sequencing – or next-generation sequencing) approaches used here can determine mtDNA damage load and precise location. This is a significant advance in mtDNA analysis and can provide not only more reproducible data but also more specific findings that generate new testable hypotheses, e.g., deletions or mutations in a specific gene.

The duration of experimental diabetes in this study, (3 months), cannot support or oppose the hypothesis that vascular mitochondrial changes occur later in the disease process. Diabetes-induced retinal vascular mtDNA damage may reach the threshold required to cause functional changes, but currently no data is present in the literature from *in vivo* retinal endothelium with the quantitative resolution to support that conclusion. Our whole retina data does include endothelial cells, but these endothelial cells are a small minority of cells analyzed and the whole retina data does not show increased damage. Detailed longitudinal studies using quantitative approaches, such as presented here, as opposed to qualitative assessments, and of specific cellular populations could determine if, when, and where mtDNA damage is present in the diabetic retina. However, the importance/relevance of mitochondrial damage and dysfunction late in the neural disease process is unclear, because the deficits in neural retinal function are already manifested. The potential mitochondrial dysfunction in later disease time points may develop secondarily to neuronal dysfunction, where breakdown of the neurovascular retina unit induces endothelial cell dysfunction and capillary cell loss (Lynch and Abramoff 2017). Interestingly, antioxidant treatments and pharmacological interventions that may support mitochondrial function are successful in reducing retinal deficits observed with diabetes (Alam *et al.* 2015). Our data do not refute the presence of reactive oxygen species or superoxide elements in the diabetic retina as increases in beta oxidation and antioxidant proteins demonstrate a response to altered metabolism and potential increased oxidative stress, but our data do not support the hypothesis that these are oxidatively damaging neural retinal mtDNA and inducing dysfunction. Longitudinal analysis of mtDNA adducts may be needed to fully assess oxidative damage over-time in the diabetic retina to determine if they manifest as functional mutations. A recent report suggests that short-term diabetes induces mitochondrial activity maintenance through prevention of oxidative stress and not dysfunction (Osorio-Paz *et al.* 2015). Therefore, it is reasonable to postulate that reducing the amount of potentially damaging molecules through pharmacological inhibition could benefit diabetic retinal function and mitigate DR progression in the absence of mitochondrial dysfunction and mtDNA damage. The benefit of antioxidants and pharmacological boosting of mitochondrial function in the diabetic retina is not evidence of oxidatively damaged mitochondria or mtDNA. If indeed mitochondrial dysfunction does induce capillary cell loss after initial retinal neural deficits, administration of antioxidant drugs could inhibit further breakdown of the neurovascular unit, but would not be useful for inhibiting the initial neural deficits of DR that precede the vascular deficits observed with long-term uncontrolled diabetes. Rather, neuroprotective treatments may prevent the initial neural retina dysfunction and possibly prevent subsequent vascular damage (Hernandez *et al.* 2013). Furthermore, our results demonstrate a significant decrease in the expression of a number of proteins related to the TCA/Krebs cycle in D+I rats compared to ND and D controls. These results suggest that with diabetes the increase in beta oxidation to form acetyl-CoA through fatty acid degradation is reversed with insulin treatment. This response in the D+I animals is potentially related to our previous findings demonstrating increased fat mass in insulin-treated diabetic animals (Masser *et al.* 2014). However, this seems to be a systemic cellular response as the retinal synaptic terminals do not store fatty acids for energy.

We conclude that neural retinal deficits that occur with 3 months of hyperglycemia are not caused by mtDNA damage-induced mitochondrial dysfunction. Our results leave open the possibility that late-stage vascular DR progression is mediated by mitochondrial damage in retinal microvasculature from long-term diabetes. However, it is not clear that the mtDNA damage reported in these studies meets or exceeds frequencies that would result in functional penetrance as detailed by the threshold effect hypothesis. Rather, the neurodegeneration occurring early in DR progression may be causative of later, classical, vascular dysfunction (Lynch and Abramoff 2017). Therefore, given the interdependence of inflammation and oxidative stress (Du *et al.* 2013), we postulate that neurodegeneration and inflammation are the mediators of neural DR initiation and progression at the beginning of the DR disease process. Additionally, the presence of inflammation could be contributing to the antioxidant response observed with DR. Future work will be instrumental in deciphering the interplay of neuroinflammation and neurodegeneration in starting the sequence of retinal changes that ultimate result in vascular dysfunction and proliferation.

Data access

All fastq files are available from the NCBI Sequence Read Archive under the accession number PRJNA389563.

Acknowledgments and conflict of interest disclosure

The authors declare no potential conflicts of interest. The authors would like to thank: Dr Allison Gillaspy of the Laboratory for Molecular Biology and Cytometry Research at OUHSC for access to MiSeq sequencing instrument, Dr Muralidharan Jayaraman the Stephenson Cancer Center Cancer Functional Genomics Core Director for training and access to the Seahorse XFe96 instrument, Dr Anja Bastian for lending expertise with designing OCR measurement protocol, Dr Feng Li and Megan Stiles at the Dean McGee Eye Institute Live Animal Imaging Core for assistance and training with ERG and OCT methods, Mark Dittmar Director of the Dean McGee Eye Institute Animal Facility and staff for support with animal housing and procedures, Dr Robert E. Anderson Director of Research at Dean McGee Eye Institute and Dr Blake Hopiavuori for gracious allowance of bench space and ultracentrifuge use for synaptosome isolations as well as aid in ERG data analysis, and Steven Glansberg for assistance with figure generation. This work was supported by the National Eye Institute (R21EY024520, R01EY021716, T32EY023202, T32AG052363), the Donald W. Reynolds Foundation, the Oklahoma Nathan Shock Center of Excellence in the Biology of Aging Targeted DNA Methylation and Mitochondrial Heteroplasmy Core (P30AG050911), The Dean McGee Eye Institute Vision Cores (P30EY021725), and supported in part by an award from Harold Hamm Diabetes Center at the University of Oklahoma.

All experiments were conducted in compliance with the ARRIVE guidelines.

Supporting information

Additional Supporting Information may be found online in the supporting information tab for this article:

Figure S1. Optical coherence tomography data acquisition.

Figure S2. Electroretinogram (ERG) photopic oscillatory potentials (OP).

Figure S3. Retinal synaptosome preparation western blots.

Figure S4. Mitochondrial DNA (mtDNA) absolute copy number.

Figure S5. Schematic of *de novo* sequencing standards and quantitative validation.

Figure S6. mtDNA variants from synaptic mtDNA sequencing replication.

Figure S7. mtDNA variants from whole retina mtDNA sequencing.

Table S1. mtDNA sequencing primers.

Table S2. Animal groups and characterization.

Table S3. Retinal morphology.

Table S4. ERG A- and B-wave implicit time and amplitude.

Table S5. Proteomic data (Excel File).

Table S6. mtDNA sequencing standards.

Table S7. Retina Synaptosome mtDNA sequencing variant frequencies (Excel File).

Table S8. Re-sequencing Retina Synaptosome mtDNA sequencing variant frequencies (Excel File).

Table S9. Whole retina mtDNA sequencing variant frequencies (Excel File).

References

Abcouwer S. F. and Gardner T. W. (2014) Diabetic retinopathy: loss of neuroretinal adaptation to the diabetic metabolic environment. *Ann. N. Y. Acad. Sci.* **1311**, 174–190.

Aiello L. P. and Group D. E. R. (2014) Diabetic retinopathy and other ocular findings in the diabetes control and complications trial/epidemiology of diabetes interventions and complications study. *Diabetes Care*, **37**, 17–23.

Alam N. M., Mills W. C. T., Wong A. A., Douglas R. M., Szeto H. H. and Prusky G. T. (2015) A mitochondrial therapeutic reverses visual decline in mouse models of diabetes. *Dis. Model Mech.* **8**, 701–710.

Antonetti D. A., Barber A. J., Bronson S. K. *et al.* (2006) Diabetic retinopathy: seeing beyond glucose-induced microvascular disease. *Diabetes* **55**, 2401–2411.

Aung M. H., Kim M. K., Olson D. E., Thule P. M. and Pardue M. T. (2013) Early visual deficits in streptozotocin-induced diabetic long evans rats. *Invest. Ophthalmol. Vis. Sci.* **54**, 1370–1377.

Barchiesi A., Baccarani U., Billack B., Tell G. and Vascotto C. (2017) [Letter to the Editor] Isolation of mitochondria is necessary for precise quantification of mitochondrial DNA damage in human carcinoma samples. *Biotechniques* **62**, 13–17.

Barot M., Gokulgandhi M. R. and Mitra A. K. (2011) Mitochondrial dysfunction in retinal diseases. *Curr. Eye Res.* **36**, 1069–1077.

Benjamini Y. and Hochberg Y. (2000) On the adaptive control of the false discovery fate in multiple testing with independent statistics. *J. Educ. Behav. Stat.* **25**, 60–83.

Bixler G. V., Vanguilder H. D., Brucklacher R. M., Kimball S. R., Bronson S. K. and Freeman W. M. (2011) Chronic insulin treatment of diabetes does not fully normalize alterations in the retinal transcriptome. *BMC Med. Genomics* **4**, 40.

Brucklacher R. M., Patel K. M., VanGuilder H. D. *et al.* (2008) Whole genome assessment of the retinal response to diabetes reveals a progressive neurovascular inflammatory response. *BMC Med. Genomics* **1**, 26.

Choi S. W., Gerencser A. A. and Nicholls D. G. (2009) Bioenergetic analysis of isolated cerebrocortical nerve terminals on a microgram scale: spare respiratory capacity and stochastic mitochondrial failure. *J. Neurochem.* **109**, 1179–1191.

Du Y., Veenstra A., Palczewski K. and Kern T. S. (2013) Photoreceptor cells are major contributors to diabetes-induced oxidative stress and local inflammation in the retina. *Proc. Natl Acad. Sci. USA* **110**, 16586–16591.

Dupuis L. (2014) Mitochondrial quality control in neurodegenerative diseases. *Biochimie* **100**, 177–183.

Durham S. E., Samuels D. C., Cree L. M. and Chinnery P. F. (2007) Normal levels of wild-type mitochondrial DNA maintain cytochrome c oxidase activity for two pathogenic mitochondrial DNA mutations but not for m.3243A–>G. *Am. J. Hum. Genet.* **81**, 189–195.

Freeman W. M., Bixler G. V., Brucklacher R. M. *et al.* (2010) A multistep validation process of biomarkers for preclinical drug development. *Pharmacogenomics J.* **10**, 385–395.

Gardner T. W., Antonetti D. A., Barber A. J., LaNoue K. F. and Levison S. W. (2002) Diabetic retinopathy: more than meets the eye. *Surv. Ophthalmol.* **47**(Suppl 2), S253–S262.

Hernandez C., Garcia-Ramirez M., Corraliza L., Fernandez-Carneado J., Farrera-Sinfreu J., Ponsati B., Gonzalez-Rodriguez A., Valverde A. M. and Simo R. (2013) Topical administration of somatostatin prevents retinal neurodegeneration in experimental diabetes. *Diabetes* **62**, 2569–2578.

Jackson G. R., Scott I. U., Quillen D. A., Walter L. E. and Gardner T. W. (2012) Inner retinal visual dysfunction is a sensitive marker of non-proliferative diabetic retinopathy. *Br. J. Ophthalmol.* **96**, 699–703.

Kowluru R. A. and Abbas S. N. (2003) Diabetes-induced mitochondrial dysfunction in the retina. *Invest. Ophthalmol. Vis. Sci.* **44**, 5327–5334.

Kowluru R. A. and Mishra M. (2015) Oxidative stress, mitochondrial damage and diabetic retinopathy. *Biochim. Biophys. Acta* **1852**, 2474–2483.

Lorenzi M. and Gerhardinger C. (2001) Early cellular and molecular changes induced by diabetes in the retina. *Diabetologia* **44**, 791–804.

Lynch S. K. and Abramoff M. D. (2017) Diabetic retinopathy is a neurodegenerative disorder. *Vision. Res.* doi: 10.1016/j.visres.2017.03.003. [Epub ahead of print]

Madsen-Bouterse S. A. and Kowluru R. A. (2008) Oxidative stress and diabetic retinopathy: pathophysiological mechanisms and treatment perspectives. *Rev. Endocr. Metab. Disord.* **9**, 315–327.

Madsen-Bouterse S. A., Mohammad G., Kanwar M. and Kowluru R. A. (2010) Role of mitochondrial DNA damage in the development of diabetic retinopathy, and the metabolic memory phenomenon associated with its progression. *Antioxid. Redox Signal.* **13**, 797–805.

Masser D. R., Berg A. S. and Freeman W. M. (2013) Focused, high accuracy 5-methylcytosine quantitation with base resolution by benchtop next-generation sequencing. *Epigenetics Chromatin* **6**, 33.

Masser D. R., VanGuilder Starkey H. D., Bixler G. V., Dunton W., Bronson S. K. and Freeman W. M. (2014) Insulin treatment normalizes retinal neuroinflammation but not markers of synapse loss in diabetic rats. *Exp. Eye Res.* **125**, 95–106.

Masser D. R., Clark N. W., Van Remmen H. and Freeman W. M. (2016) Loss of the antioxidant enzyme CuZnSOD (Sod1) mimics an age-related increase in absolute mitochondrial DNA copy number in the skeletal muscle. *Age (Dordr)* **38**, 323–333.

Nakada Y., Canseco D. C., Thet S. *et al.* (2017) Hypoxia induces heart regeneration in adult mice. *Nature* **541**, 222–227.

Nathan D. M., Diabetes C., Complications Trial/Epidemiology of Diabetes I., Complications Research G., Lachin J. M., White N. H., Hainsworth D. P., Sun W. and Cleary P. A. (2015) Effect of intensive diabetes therapy on the progression of diabetic retinopathy in patients with type 1 diabetes: 18 years of follow-up in the DCCT/EDIC. *Diabetes*, **64**, 631–642.

Osorio-Paz I., Uribe-Carvajal S. and Salceda R. (2015) In the early stages of diabetes, rat retinal mitochondria undergo mild uncoupling due to UCP2 activity. *PLoS ONE* **10**, e0122727.

Pardue M. T., Barnes C. S., Kim M. K., Aung M. H., Amarnath R., Olson D. E. and Thule P. M. (2014) Rodent hyperglycemia-induced inner retinal deficits are mirrored in human diabetes. *Transl. Vis. Sci. Technol.* **3**, 6.

Santos J. M., Tewari S. and Kowluru R. A. (2012) A compensatory mechanism protects retinal mitochondria from initial insult in diabetic retinopathy. *Free Radic. Biol. Med.* **53**, 1729–1737.

Sennlaub F., Valamanesh F., Vazquez-Tello A. *et al.* (2003) Cyclooxygenase-2 in human and experimental ischemic proliferative retinopathy. *Circulation* **108**, 198–204.

Sheng Z. H. and Cai Q. (2012) Mitochondrial transport in neurons: impact on synaptic homeostasis and neurodegeneration. *Nat. Rev. Neurosci.* **13**, 77–93.

Sohn E. H., van Dijk H. W., Jiao C. *et al.* (2016) Retinal neurodegeneration may precede microvascular changes characteristic of diabetic retinopathy in diabetes mellitus. *Proc. Natl Acad. Sci. USA* **113**, E2655–E2664.

Stewart J. B. and Chinnery P. F. (2015) The dynamics of mitochondrial DNA heteroplasmy: implications for human health and disease. *Nat. Rev. Genet.* **16**, 530–542.

Stitt A. W., Curtis T. M., Chen M. *et al.* (2016) The progress in understanding and treatment of diabetic retinopathy. *Prog. Retin. Eye Res.* **51**, 156–186.

Suresh K. (2011) An overview of randomization techniques: an unbiased assessment of outcome in clinical research. *J. Hum. Reprod. Sci.* **4**, 8–11.

Taylor R. W. and Turnbull D. M. (2005) Mitochondrial DNA mutations in human disease. *Nat. Rev. Genet.* **6**, 389–402.

Tewari S., Santos J. M. and Kowluru R. A. (2012) Damaged mitochondrial DNA replication system and the development of diabetic retinopathy. *Antioxid. Redox Signal.* **17**, 492–504.

Valente W. J., Ericson N. G., Long A. S., White P. A., Marchetti F. and Bielas J. H. (2016) Mitochondrial DNA exhibits resistance to induced point and deletion mutations. *Nucleic Acids Res.* **44**, 8513–8524.

VanGuilder H. D., Brucklacher R. M., Patel K., Ellis R. W., Freeman W. M. and Barber A. J. (2008) Diabetes downregulates presynaptic proteins and reduces basal synapsin I phosphorylation in rat retina. *Eur. J. Neurosci.* **28**, 1–11.

VanGuilder H. D., Bixler G. V., Kutzler L., Brucklacher R. M., Bronson S. K., Kimball S. R. and Freeman W. M. (2011) Multi-modal proteomic analysis of retinal protein expression alterations in a rat model of diabetic retinopathy. *PLoS ONE* **6**, e16271.

Vaziri K., Schwartz S. G., Relhan N., Kishor K. S. and Flynn H. W., Jr (2015) New therapeutic approaches in diabetic retinopathy. *Rev. Diabet. Stud.* **12**, 196–210.

Ye K., Lu J., Ma F., Keinan A. and Gu Z. (2014) Extensive pathogenicity of mitochondrial heteroplasmy in healthy human individuals. *Proc. Natl Acad. Sci. USA* **111**, 10654–10659.

Zhong Q. and Kowluru R. A. (2011) Diabetic retinopathy and damage to mitochondrial structure and transport machinery. *Invest. Ophthalmol. Vis. Sci.* **52**, 8739–8746.